

Advances in Basic and Applied Sciences



journal homepage: https://abas.journals.ekb.eg/

Molecular docking, Molecular dynamics simulation and MMPBSA studies on potential lead compounds fighting NSP6 of SARS-CoV-2

Mohammed Mostafa Salama^{1*}, Medhat Wahba Shafaa¹, Mohamed El-Sayed El-Nagdy¹, Mohamed El-Sayed Hasan^{2,3}

ARTICLE INFO

Article history:

Received 13 August 2025 Received in revised form 6 September 2025 Accepted 10 September 2025 Available online 25 October 2025

doi: 10.21608/ABAS.2025.410458.1072

Keywords: SARS-CoV-2; NSP6; in silico; Molecular dynamic simulation; Molecular docking; MMPBSA; vaccine testing.

Abstract

Background: The non-structural protein 6 (NSP6) in SARS-CoV-2 is one of the most fascinating NSPs for drug targeting, because of its decisive role in the replication of the virus inside the host cells. This study aimed to predict a fine model of the tertiary structure of the NSP6 and to find a vaccine candidate to fight the NSP6.

Methods: The AlphaFold 3 server was used in the prediction of the tertiary structure of the protein, then the model was refined using the DeepRefiner server, and finally, the quality of the refined model was estimated using the SAVES server. A full library of the available chemical ligands was downloaded from the ZINC20 database, and then these ligands were docked against the NSP6 protein. The physicochemical and drug likeness and the toxicity of the picked-up ligands were tested using SwissParam, Swiss-ADME, ProTox III, and ADMET-AI servers. The ligand complex with the NSP6 was subjected to Molecular dynamics simulation to assess its interactions with the protein through RMSD, RMSF, SASA, Rg, H-bonds, and free energy studies. The MD simulations were run a 100 ns time to study the changes of the trajectories and the parameters of the complexes compared to the NSP6-apo protein.

Results: The AlphaFold server produced a high-quality model, and after refinement, the SAVES server indicated that the structure had a quality percent of 99.94%. The docking process selected two ligands, ZINC0117742510 and

¹ Helwan University, Faculty of Science, Physics Department, Medical Biophysics Division, Cairo, Egypt.

² University of Sadat City, Genetic Engineering and Biotechnology Research Institute, Bioinformatics Department, Sadat City 32897, Egypt.

³ Borg Al Arab Technological University (BATU), Faculty of Applied Health Science, Department of Health Information Technology, Borg Al Arab, Egypt.

ZINC1500127684, that are suitable as potential inhibitors. The RMSD results of the NSP6-ZINC0117742510 and the NSP6-ZINC1500127684 complexes revealed that they reached stability in the 2 to 2.6 nm. The MD simulations analysis revealed that the NSP6-ZINC1500127684 and the NSP6-ZINC0117742510 proved minimal deviations and suitable stability compared to the NSP6-apo protein. The Molecular Mechanics Poisson—Boltzmann Surface Area (MMPBSA) analysis indicated that the NSP6-ZINC1500127684 complex had a lower binding energy than the NSP6-ZINC0117742510.

Conclusion: Therefore, ZINC0117742510 and ZINC1500127684 ligands were proven as potential inhibitors against the SARS-CoV-2 NSP6 protein.

1. Introduction

A wide pandemic invasion caused by the novel Severe Acute Respiratory Syndrome Coronavirus 2 (SARS-CoV-2), which infected and caused deaths of millions all over the world, attracted the attention of researchers to discover the new virus [1,2]. The genome of SARS-CoV-2 embraces 26 to 32 kb, sectioned into 11 open reading frames (ORFs), that encode 9680 amino acid polyproteins. ORF1 comprises more than 67% of the full genome of SARS-CoV-2 and encodes 16 non-structural proteins (NSPs), which are important in the replication and transcription processes of the virus inside the host cells. The other ORFs encode the structural and accessory proteins. The encoded structural proteins are the envelope (E), spike (S), nucleocapsid (N), and membrane (M) proteins [3-5].

The NSP6 protein is found to have an important function in the process of viral replication, so it is considered one of the most attractive NSPs in SARS-CoV-2. Until now, there is no crystalized tertiary structure of the NSP6, therefore, researchers are using bioinformatic tools to predict the tertiary structure of the NSP6 in their studies [6,7]. The NSP6 protein consists of 290 amino acid residues. Studies have found that it takes part in the cycle of infection, protection, and replication of the SARS-CoV-2. In addition, it is found to have a vital role in the replication-transcription complexes (RTCs) assembly with NSP3 and NSP4 by increasing the double-membrane vesicles (DMVs) production [8-12]. Furthermore, it interacts with the sigma receptor of the endoplasmic reticulum (ER), which affects the performance of the ER [13-15].

Bioinformatics plays an essential role in biomedical research, including drug and vaccine development. Compared to traditional methods such as NMR spectroscopy and X-ray crystallography, bioinformatics tools such as tertiary structure predictions could offer an alternative with high-cost reduction and time savings in addition to the acceleration of drug discovery [16-19]. Many researchers used bioinformatics in their studies about SARS-CoV-2 and the NSP6 protein [6-10].

Molecular dynamics simulation (MD simulations) is a process that uses objects to analyze the dynamics of macromolecules in a simulated, well-controlled biophysical environment. Through this computational process, the physical relations in the system are determined via detection of the flexibility of the complexes along the simulation time. Additionally, the MD simulations process aims to study the interactions between the ligand and the active sites of the NSP6 protein and estimating the stability of these interactions [15].

In this study, we aimed to predict a suitable vaccine candidate against the NSP6 protein of SARS-CoV-2 using many bioinformatics tools like protein structure prediction, molecular docking, molecular dynamic simulations, Molecular Mechanics Poisson–Boltzmann Surface Area (MMPBSA), and ADMET prediction.

2. Methods

2.1. Structure modelling of the NSP6 protein

The PSIPRED server was used in the prediction of the secondary structure of the protein [20]. The AlphaFold 3 server was employed to predict the tertiary structure of the NSP6. AlphaFold uses a deep neural network in the prediction process through DeepMind algorithms [21-23]. Then the DeepRefiner server was used to refine the produced model of the NSP6 protein to provide a higher quality model [24]. Finally, we used the SAVES server to predict and estimate the quality of the refined tertiary structure model of the NSP6 [25].

2.2. Virtual screening and molecular Docking

The molecular docking process was used to predict the possible ligand candidates through the binding affinity between the ligands and the NSP6 protein. The SwissDock server was used in molecular docking, which is based on the Attracting cavities (AC) and the Autodock Vina docking engines [26]. The ZINC20 database library was used as the ligand library in the docking studies. It is an ultra-large-scale database that includes more than a billion possible candidates that are suitable for docking [27]. The SwissDock server was used to estimate the binding affinities in the protein-ligand complexes, in addition to rich information about the interactions in the complex. The scoring function uses CHARMM force field, generating one random initial condition, and default number of dockings poses to reach the highest quality results [26,28].

2.3. MD simulation

MD simulation is an important process to study the stability and the flexibility of the protein-ligand complexes, in which the complex was centred in a cubic box with 10 Å length of the edges. The TIP3P water molecule model was used to surround the complex inside the box. To maintain the salt concentration inside the box, 0.15M of Na⁺ and Cl⁻ ions were added to the box. Moreover, we used Particle-Ewald summation to estimate the electrostatic interactions, and 10 Å cut-off to estimate the Van der Waals. The prepared system was energy minimized for 50000 steps using suitable algorithms, then it was subjected to NVT and NPT equilibrium processes for 100 ps per step. Finally, the MD simulation production started for 100 ns with a snapping rate every 10 ps to use in the analysis. We used the GROMACS-2021.3 package for the run and the analysis of the MD simulation, root mean square fluctuation (RMSF), the protein root mean square deviation (RMSD), solvent accessible surface area (SASA), radius of gyration (RG), and hydrogen bonding (H-Bond) [29-39]. The MD simulation for the protein-ligand complexes and the analysis processes were applied on the Bibliotheca Alexandrina Supercomputing unit [29-31].

2.4. Binding free energy estimation

The Molecular Mechanics Poisson–Boltzmann Surface Area (MM-PBSA) was accustomed to estimate the docking values, the bonds and their energies, and the binding affinities of the ligands. Also, it accurately estimates the binding free energies of the protein-ligand complex. In addition, it was used to estimate the potential interactions and binding sites. The binding free energies of the protein-ligand complexes were estimated through:

 $\Delta G_{binding} = G_{complex} - G_{protein} - G_{ligand}$,

G_{complex}: the free energy of the protein-ligand complex

 $G_{protein}$: the free energy of protein G_{ligand} : the free energy of ligand.

The MM-PBSA results were used in the estimation of the binding of protein-ligand complexes and to estimate the potential interactions and binding sites. We used the GROMACS-2021.3 package for the run and the analysis of the MM-PBSA with frame every 100 ps [40 -44].

2.5. Physicochemical and Drug-Likeness Properties

To validate the ligand as a possible vaccine, we have to predict the absorption, metabolism, distribution, and excretion of the ligand inside the body (ADME). We used the Swiss-ADME server to predict the drug-likeness and physicochemical properties of the ligands. Swiss-ADME server could estimate the molecular weight, H-bond donors and acceptors, and Lipinski's rule of 5, in addition to the BOILEG-Egg, iLOGp, and the Bioavailability radar [45]. Furthemore, we used ProTox III and ADMET-AI servers to predict the drug-like properties of the ligands [46 - 47].

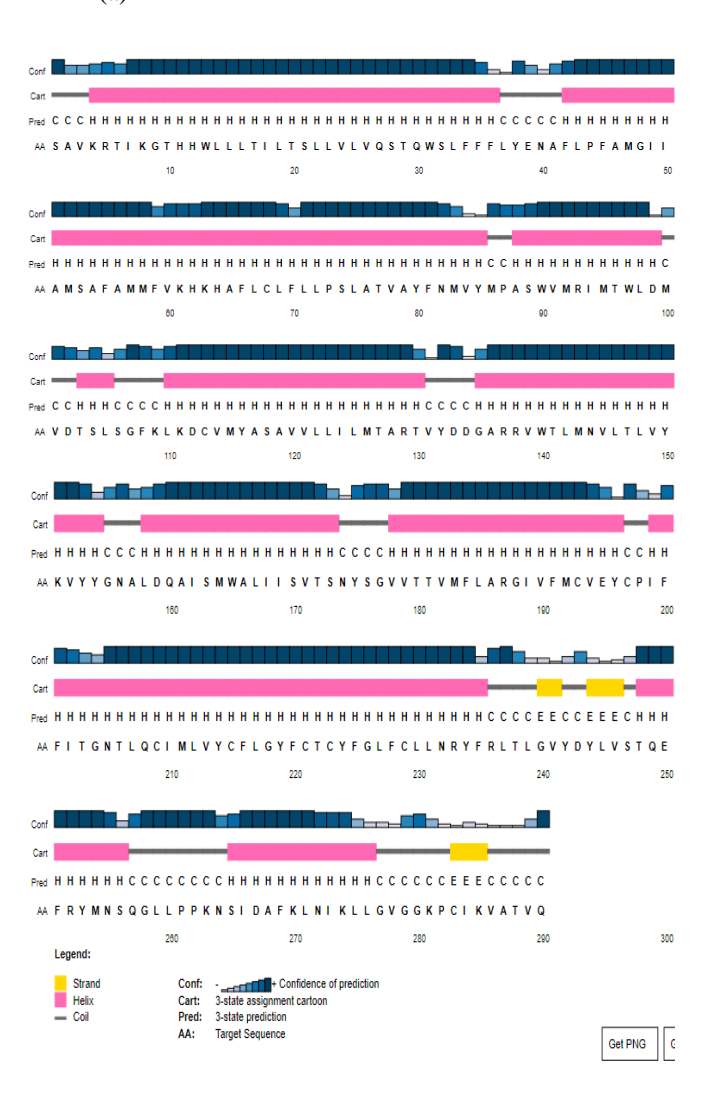
3. Results

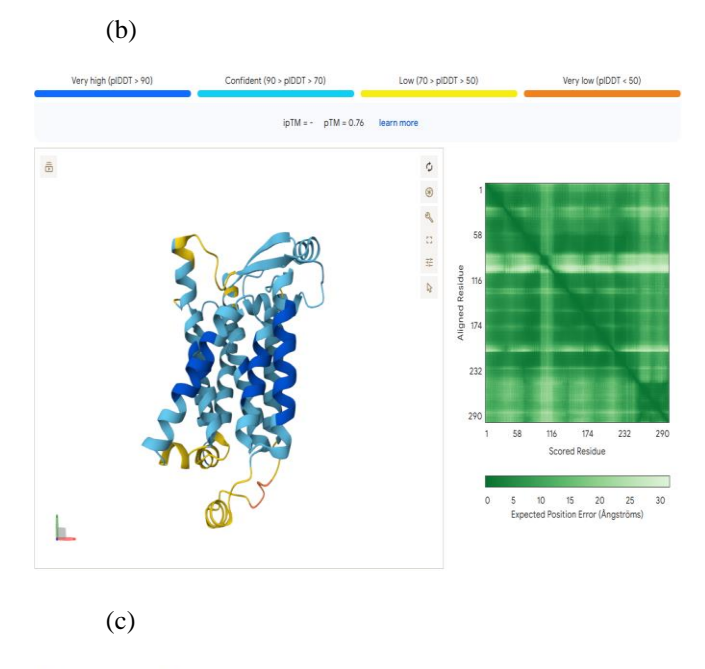
3.1. Structure modelling of the NSP6 protein

PSIPRED server was used in the prediction of the secondary structure of the NSP6 protein; the results showed that the structure may be 77.93% $\alpha\text{-helices}, 19.31\%$ coils, and 2.76% $\beta\text{-strands}$ (Figure 1a). The AlphaFold 3 server was used in the prediction of the tertiary structure of the NSP6 protein (Figure 1b). After that, the DeepRefiner server was used to refine the predicted model to increase its quality, and finally, the quality of the refined model was estimated using the SAVES server.

The results indicated that the structure of the protein is composed of two antiparallel beta sheets, 16 turns, and 14 alpha helices. Additionally, it includes 8 transmembrane helices. According to the SAVES server, the refined model has an overall quality of 99.64% with 94.4% in the core region, and 5.6% in the allowed regions, with no residues in the disallowed region in the Ramachandran plot (Figure 1).

(a)





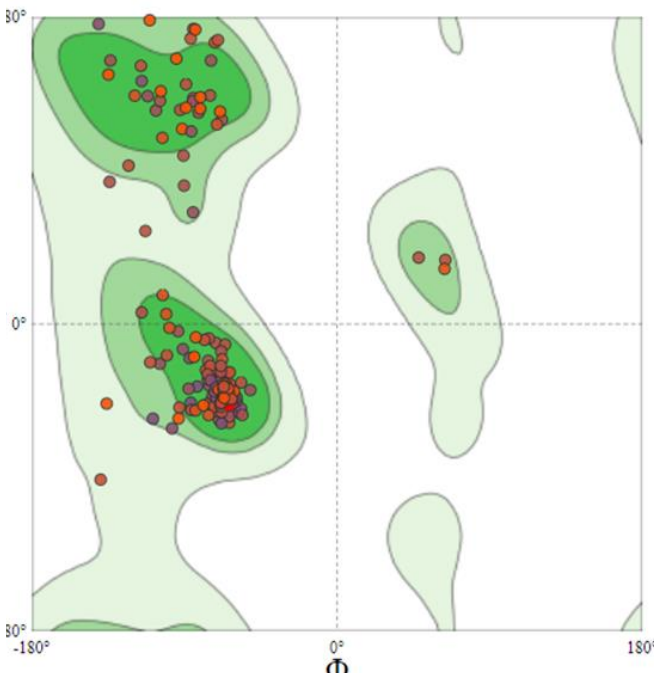


Figure 1: (a) The predicted secondary structure of the NSP6 protein. (b) The ribbon view of the best-predicted model. (c) Ramachandran plot.

3.2. Virtual Screening and Molecular Docking

To predict the binding affinity between the NSP6 protein with the candidate ligands, we have to perform the molecular docking. A library of 2.9 million ligands from the ZINC20 database was docked against the NSP6 using the SwissDock server, which applies the Attracting Cavities and Autodock Vina docking engines. Discovery studio

2021client was used to visualize the protein-ligand complexes. Through comparing the AC and SwissParam Scores, two ligands have the lowest scores (Table 1), with docking sites shown in Figure 2.

Table 1. A list of top-scored drug-like molecules resulted from molecular docking analyses using the SwissParam SwissDock.

ZINC database ID	0117742510	1500127684
Chemical structure		
AC Score	-97.85	-94.64
SwissParam Score	-7.48	-7.80

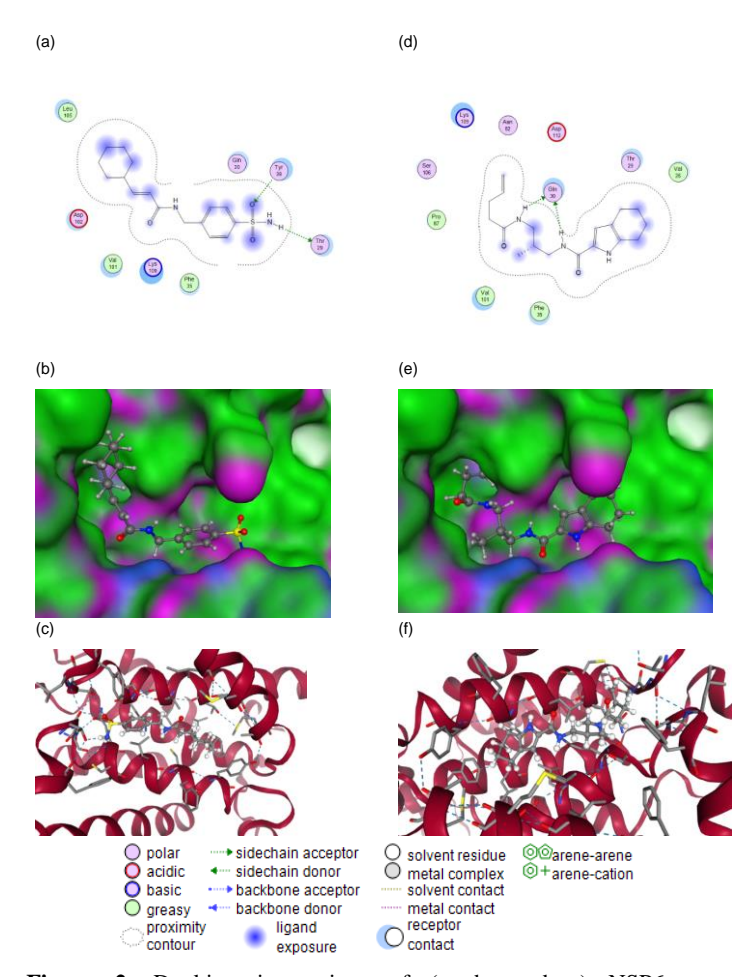


Figure 2. Docking interactions of (a, b, and c) NSP6-ZINC0117742510, and (d, e, and f) NSP6-ZINC1500127684.

3.3. Drug-Likeness and Physicochemical Analysis

The Swiss-ADME server was applied in the prediction of the ADMET parameters of the candidate ligands, in which it assesses the drug-likeness, molecular weight, hydrophobicity (logP), and Lipinski's rule of five of the ligands. The ligands showed that they have a molecular weight less than 350 g/mol, no violations of Lipinski's rules, and log P values less than 5 (Table 2).

Table 2. Drug-likeness characteristics of the chosen drug-like complexes obtained using the Swiss-ADME server.

ZINC database ID	0117742510	1500127684
Molecular formula	C18H27N3O2	C16H22N2O3S
Molecular weight (g/mol)	317.43	322.42
No. of H-bond acceptors	2	4
No. of H-bond donors	3	2
LogP (octanol/water partition coefficient)	2.67	2.22
Lipinski's no. of violations	0	0
Ghose's no. of violations	0	0
Veber's no. of violations	0	0
Bioavailability Score	0.55	0.55
PAINS no. of alerts	0	0

3.4. Toxicity prediction

To evaluate the toxicity of the ligands, we used the ProTox III and ADMET-AI servers. The results indicated that the ligands didn't have any positive results towards cardiotoxicity, clinical toxicity, nephrotoxicity, blood-brain barrier (BBB) penetration, carcinogenicity, cytotoxicity, mutagenicity, or nutritional toxicity (Tables 3:7).

Table 3. Physicochemical properties of the selected drug-like complexes obtained using the ADMET-AI server.

ZINC database ID	0117742510	1500127684	Units
Molecular Weight	317.43	322.43	Dalton
LogP	2.34	2.09	log-
			ratio
Hydrogen Bond	2.00	3.00	#
Acceptors			
Hydrogen Bond	3.00	2.00	#
<u>Donors</u>			
Lipinski Rule of 5	4.00	4.00	# of 4
Quantitative Estimate	0.64	0.81	-
of Druglikeness (QED)			
Stereo Centers	1.00	0.00	#
Topological Polar	73.99	89.26	$\mathring{\mathbf{A}}^2$
Surface Area (TPSA)			

Table 4. Absorption properties of the chosen drug-like complexes obtained using the ADMET-AI server.

ZINC database ID	0117742510	1500127684	Units
Human Intestinal Absorption	1.00	1.00	-
<u>Oral</u> <u>Bioavailability</u>	0.83	0.86	-
Aqueous Solubility	-3.26	-3.07	log(mol/L)
<u>Lipophilicity</u>	2.71	1.73	log-ratio
Hydration Free Energy	-10.53	-8.14	kcal/mol
Cell Effective Permeability	-5.06	-4.80	log(10 ⁻ ⁶ cm/s)
PAMPA Permeability	0.88	0.79	-
P-glycoprotein Inhibition	0.16	0.19	-

Table 5. Distribution properties of the chosen drug-like complexes obtained using the ADMET-AI server.

ZINC database ID	0117742510	1500127684	Units
Blood-Brain Barrier Penetration	0.88	0.86	-
Plasma Protein Binding Rate	79.91	88.35	%
Volume of Distribution at Steady State	2.88	0.00	L/kg

Table 6. Metabolism properties of the chosen drug-like complexes obtained using the ADMET-AI server

ZINC database ID	0117742510	1500127684	Units
CYP1A2 Inhibition	0.47	0.06	-
CYP2C19 Inhibition	0.44	0.33	-
CYP2C9 Inhibition	0.08	0.05	-
CYP2D6 Inhibition	0.21	0.05	-
CYP3A4 Inhibition	0.54	0.34	-
CYP2C9 Substrate	0.20	0.50	-
CYP2D6 Substrate	0.44	0.11	-
CYP3A4 Substrate	0.71	0.48	-

Table 7. Excretion properties of the chosen drug-like complexes obtained using the ADMET-AI server.

ZINC database ID	011774251 0	150012768 4	Units
<u>Half Life</u>	3.23	0.00	hr
Drug Clearance (Hepatocyte)	58.19	42.44	uL/min/10 ⁶ cell s
Drug Clearance (Microsome)	38.19	35.10	uL/min/mg

3.5. Molecular Dynamics Simulations

Molecular dynamics simulation was performed using GROMACS version 2021.3. The simulation at 100 ns time was applied on the apo protein and the NSP6-ligand complexes, then the changes in the trajectories were studied and matched to the apo protein.

3.5.1. RMSD

Evaluation of the conformational and structural constancy of the NSP6-apo and the NSP6-ligand complexes can be reviewed using the RMSD of the backbone of the protein against the duration of simulation (Figure 3). The NSP6-apo protein established a sharp rise in the RMSD values up to 5 ns, then it became stable within 0.2 and 0.35 nm over the period. The NSP6-ZINC0117742510 and the NSP6-ZINC1500127684 showed a continual increase in the RMSD up to 50 ns, then reached stability within 2 to 2.6 nm over the period.

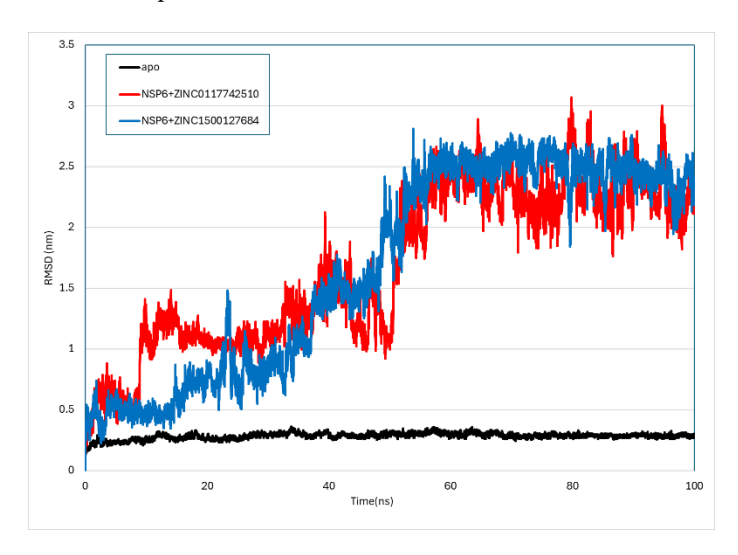


Figure 3. RMSD chart of NSP6-ZINC complexes generated through MD simulations at 100 ns.

3.5.2. RMSF

RMSF is used to compare the average estimation of the displacement of a group of atoms or a specific structure with a reference structure. We used RMSF to compare the flexibility of the residues and backbone of the complexes along the timescale of simulation 100 ns (Figure 4) and the average of the RMSF values is calculated (Table 8) focusing on the residue regions 30 - 50, 80-100, and 170-200. Compared to the NSP6-apo, the NSP6-ZINC1500127684 had lower and a leftward shift fluctuation in the 30-50 and 80-100 regions. While the NSP6-ZINC0117742510 exhibited higher fluctuations in the 80-100 and 80-100 regions, but lower in the 170-200 region.

Table 8. The average RMSF values for the NSP6 complexes with ZINC compounds.

Complex	Average RMSF (nm)
NSP6-ZINC0117742510	0.12 ± 0.08
NSP6-ZINC1500127684	0.11 ± 0.06

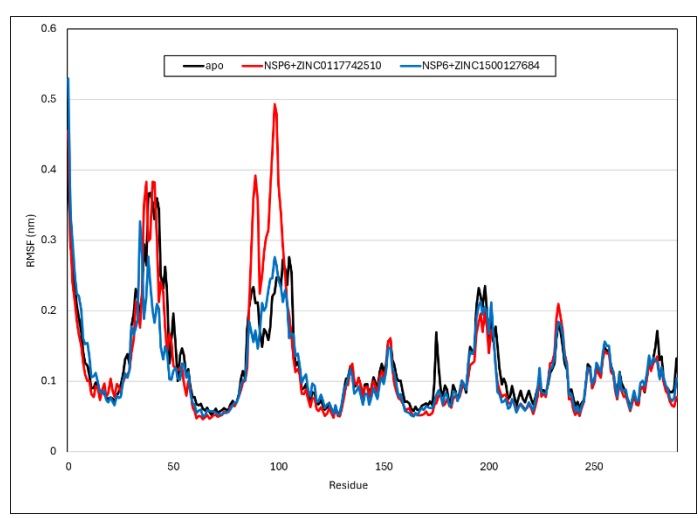


Figure 4. RMSF chart of the NSP6-ZINC complexes resulted through MD simulations at 100 ns.

3.5.3. Radius of Gyration

Radius of gyration (Rg) was used in the approximation of the compactness and integrity of the NSP6-apo, NSP6-ZINC0117742510, and NSP6-ZINC1500127684 complexes' structure to have a precise evaluation of their stability. The average Rg values for the NSP6-apo, NSP6-ZINC0117742510, and NSP6-ZINC1500127684 from 0 to 100 ns are 2.04 ± 0.01 , 2.04 ± 0.01 and 2.03 ± 0.01 nm², respectively (Figure 5).

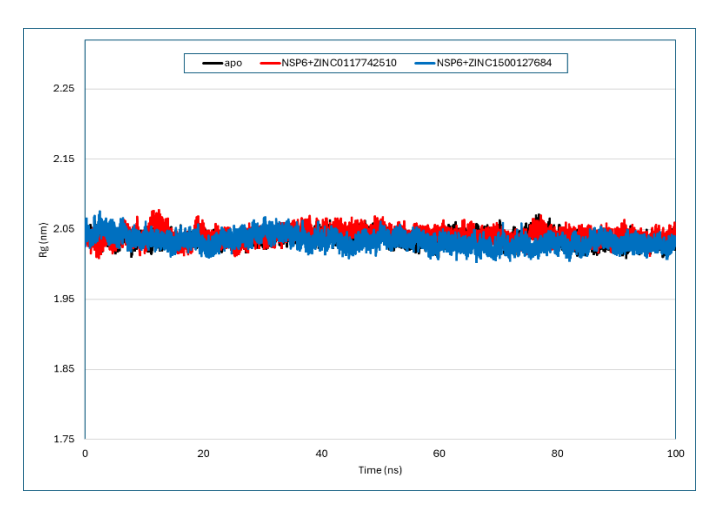


Figure 5. Rg chart of the NSP6-ZINC complexes resulted through MD simulations at 100 ns.

3.5.4. SASA Analysis

The solvent-accessible surface area (SASA) was used to predict the exposed area of the NSP6-ligand complexes and the NSP6-apo that can interact with the surrounding solvents. The changes of the SASA of the three structures alongside the simulation from 0 to 100 ns were detected and analysed (Figure 6). The average SASA values for the NSP6-apo, NSP6-ZINC0117742510, and NSP6-ZINC1500127684 from 0 to 100 ns are 163.7±2.65, 162.8±2.36 and 162.3±2.68 nm², respectively.

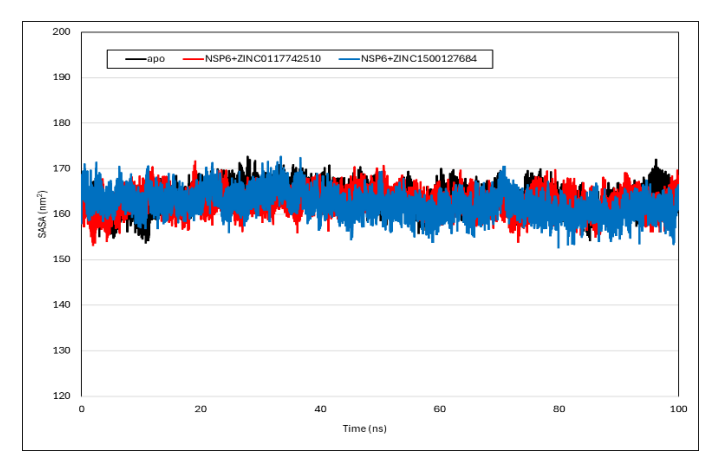


Figure 6. SASA chart of the NSP6-ZINC complexes resulted through MD simulations at 100 ns.

3.5.5. Molecular Interactions Analysis

The hydrogen bonds maintain the strength of the protein-ligand complex. We used the CHAARM force field to estimate the hydrogen bonds in the complexes alongside the simulation time (Figure 7). The NSP6-ZINC1500127684 has the highest number of hydrogen bonds with 8483 bonds, while the NSP6-ZINC0117742510 has 3338 Bonds, with 0.85, and 0.33 average hydrogen bonds per frame respectively.

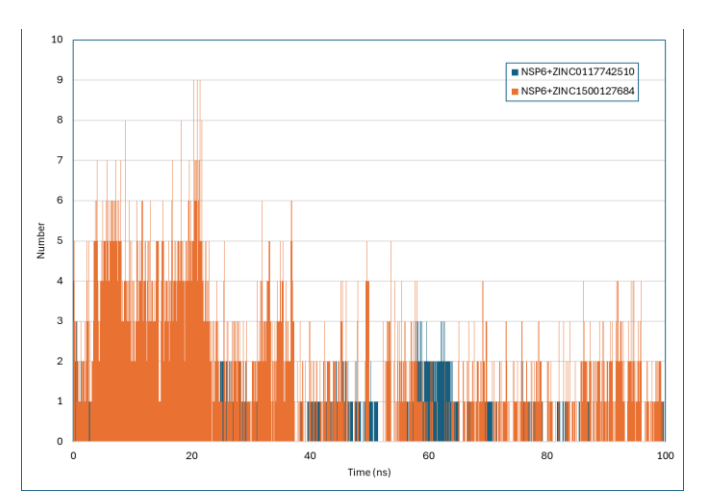


Figure 7. H-bond chart of the NSP6-ZINC complexes resulted through MD simulations at 100 ns.

3.5.6. MM-PBSA Analysis

To increase confidence in the NSO6-ligand complexes, the physical energies between the ligands and the NSP6 must be analysed. Following the MD simulation, MMPBSA analysis is needed to detect the best pose of docking of the protein-ligand complex. MMPBSA is used to analyse the energies controlling the stability of the NSP6-ligand complexes (Table 9). The NSP6-ZINC1500127684 complex was realized to have the lowest VdW, Electrostatic, and Binding energy. The free energy situation of the residues in the complexes was analysed per residue (Figure 8).

Table 9. The estimation of various energies observed in the NSP6+ligand systems.

Tibl O Tiguia	systems.			
	Van der	Electrostat	Polar	Binding
Complex	Waals	ic	Solvation	Energy
Complex	Energy	Energy	Energy	(kcal/M
	(kcal/Mol)	(kcal/Mol)	(kcal/Mol)	ol)
NSP6-	-24.72	-8	14.78	-17.93
ZINC0117				
742510				
NSP6-	-26.36	-13.89	19.14	-21.11
ZINC1500				
127684				

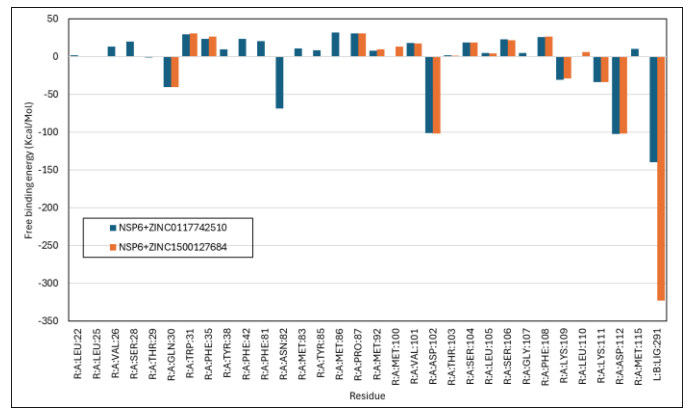


Figure 8. Binding free energy decomposition of the NSP6-ZINC-0117742510 and NSP6-ZINC-1500127684.

4. Discussions

The NSP6 protein is an important objective in fighting SARS-CoV-2; however, the absence of a verified tertiary structure motivates researchers to predict its tertiary structure and a vaccine to eliminate its role. AlphaFold server was used to predict the tertiary structure, then the model was refined using DeepRefiner, and finally the excellence of the refined model was assessed using the SAVES server and the quality percent were 99.94% the structure was in the core region with 5.6% in the allowed region of the Ramachandran plot, which reveals the quality of the predicted model.

A full library of suitable ligands was downloaded from the ZINC20 database; the library included more than a billion possible ligands. First, the ligands in the library were docked to the NSP6, SwissDock server, which is based on the Attracting cavities (AC) and Autodock Vina docking engines were used for docking studies. Based on the AC and SwissParam Scores, 2 ligands have the lowest scores. The physicochemical and drug likeness of these ligands were analyzed using the Swiss-ADME server, and the toxicity of ligands was analyzed using ProTox III and ADMET-AI servers. The ADMET and toxicity studies revealed that both ligands have MW less than 380 g/mol, with no Lipinski, Ghose and Veber violations; furthermore, they have suitable toxicity parameters that support the ligands.

The ligand complex with the NSP6 was subjected to MD simulations study to evaluate their interactions with the protein through RMSD, RMSF, SASA, Rg, H-bonds, and free energy studies. The MD simulations were run at 100 ns time function to study the changes of the trajectories and the parameters of the complexes compared to the NSP6-apo. The RMSD of the NSP6-APO complex increased sharply up to 5 ns before stabilizing between 0.2 and 0.35 nm. The NSP6-ZINC0117742510 and the NSP6-ZINC1500127684 showed a continual increase in the RMSD up to 50 ns, then reached stability within 2 to 2.6 nm over the period.

The average of the RMSF values for the NSP6-ZINC1500127684 and the NSP6-ZINC0117742510 complexes presented that the NSP6-ZINC1500127684 complex has the lowest RMSF average with 0.11 ± 0.06 nm, while the NSP6-ZINC0117742510 was 0.12 ± 0.08 nm, which indicates the greater stability of the NSP6-ZINC1500127684 complex. The average Rg values for the NSP6-ZINC0117742510, NSP6-apo, and NSP6-ZINC1500127684 from 0 to 100 ns are 2.04±0.01, 2.04±0.01 and 2.03±0.01 nm², respectively, which reveals that the complexes exhibited the same performance as the NSP6-apo, indicating that the ligands don't alter the stability or the dynamics of the protein.

The changes of the SASA of the three structures alongside the simulation from 0 to 100 ns were detected and analysed. The average SASA values for the NSP6-apo, NSP6-ZINC0117742510, and NSP6-ZINC1500127684 from 0 to 100 ns are 163.7±2.65, 162.8±2.36 and 162.3±2.68 nm², respectively, which indicates that the NSP6-

ZINC1500127684 provided the lowest SASA. The estimation of H-bonds of the NSP6-ZINC1500127684, and the NSP6-ZINC0117742510 complexes was 8483 and 3338 bonds, respectively, which indicated that the NSP6-ZINC1500127684 is the strongest in binding and has more binding affinity.

To analyze the binding energies of the NSP6-ZINC1500127684 and the NSP6-ZINC0117742510 complexes, we used the MMPBSA analyses. The results displayed that the NSP6-ZINC1500127684 complex has the lowest binding energy score with -21.11 kcal/Mol, while the Van der Waals interactions play a higher significant effect than the electrostatic contacts, indicating the best stability among the complexes. According to the results and the analysis of RMSD, RMSF, Rg, SASA, H-bonds, and MMPBSA, ZINC0117742510 and ZINC1500127684 ligands proved a promising potential as a candidate vaccine against the SARS-CoV-2 NSP6 protein, with a slight advantage for ZINC1500127684 over ZINC0117742510.

Comparing these results with the work of Ahmed Abdelkader and colleagues [8], who investigated the suitability of ligands from Northern African Natural Products Database (NANPDB), FDA-approved drugs (DrugBank), and South African Natural Compounds Database (SANCDB) products, the methods used in the study were the same as in this paper; moreover, we applied the MMPBSA analysis, which is much slower and more expensive than the MMGBSA, which was used in their paper, but the MMPBSA reveals more accurate results [28]. In comparison, the ZINC0117742510 and ZINC1500127684 ligands revealed lower binding energies than their ligands with higher H-bonds than theirs.

Conclusion

Bioinformatics opened a new era of scientific research. Using bioinformatics, the tertiary structure model of the NSP6 protein was predicted using AlphaFold, refined, and assessed. Using the library of ZIN20 database, the ZINC20 ligands were docked and virtually screened against the NSP6 protein using the SwissDock server. ZINC0117742510 and ZINC1500127684 ligands were picked up due to their results in docking. Molecular dynamics simulations were applied to the apo protein and the NSP6-ligand complexes for 100 ns. The complexes' stability, trajectories, and flexibility were evaluated compared to the apo protein based on the analyses of RMSD, radius of gyration (Rg), SASA, and RMSF. The NSP6-ZINC1500127684 and the NSP6-ZINC0117742510 revealed minimal deviations and suitable stability compared to the NSP6-apo. The MMPBSA analysis indicated that the NSP6-ZINC1500127684 complex had a lower binding energy than the NSP6-ZINC0117742510. Consequently, ZINC0117742510 and ZINC1500127684 were identified as promising small-molecule inhibitors against the SARS-CoV-2 NSP6 that warrant further in vitro and in vivo validation.

Acknowledgements

This study wasn't supported.

Conflicts of interest

The authors have no conflicts of interest to declare

Authors' contributions

M.E.H. designed the study. M.M.S. and M.E.H. performed the experiments, calculations and analyzed the data. M.E.H. and M.W.S. prepared figures of the results. M.M.S. and M.E.N. wrote the manuscript with the contributions of M.E.H., M.E.N. and M.W.S. All authors read and approved the final manuscript.

References

- [1] C. Huang, Y. Wang, X. Li, L. Ren, J. Zhao, Y. Hu, L. Zhang, G. Fan, J. Xu, X. Gu, Clinical features of patients infected with 2019 novel coronavirus in Wuhan, China, The Lancet 395 (2020) 497–506.
- [2] Q. Li, X. Guan, P. Wu, X. Wang, L. Zhou, Y. Tong, R. Ren, K.S. Leung, E.H. Lau, J.Y. Wong, Early transmission dynamics in Wuhan, China, of novel coronavirus–infected pneumonia, N. Engl. J. Med. 382 (2020) 1199–1207.
- [3] Guo YR, Cao QD, Hong ZS, Tan YY, Chen SD, Jin HJ, Tan KS, Wang DY, Yan Y. The origin, transmission and clinical therapies on coronavirus disease 2019 (COVID-19) outbreak an update on the status. Mil Med Res. 2020 Mar 13;7(1):11.
- [4] Zhou, P., Yang, XL., Wang, XG. et al. A pneumonia outbreak associated with a new coronavirus of probable bat origin. Nature 579, 270–273 (2020)
- [5] Lu, R., Zhao, X., Li, J., et al., 2020. Genomic characterization and epidemiology of 2019 novel coronavirus: implications for virus origins and receptor binding. Lancet. S0140-6736 (20), 30251– 30258.
- [6] Abdelkader A, Elzemrany AA, El-Nadi M, Elsabbagh SA, Shehata MA, Eldehna WM, El-Hadidi M, Ibrahim TM. In-Silico targeting of SARS-CoV-2 NSP6 for drug and natural products repurposing. Virology. 2022 Aug;573:96-110.
- [7] Lubin, J.H., Zardecki, C., Dolan, E.M., Lu, C., Shen, Z., et al., 2020. Evolution of the SARS-CoV-2 Proteome in Three Dimensions (3D) during the First Six Months of the COVID-19 Pandemic. bioRxiv.
- [8] Pandey, P., Prasad, K., Prakash, A., Kumar, V., 2020. Insights into the biased activity of dextromethorphan and haloperidol toward SARS-CoV-2 NSP6: in silico binding mechanistic analysis. J. Mol. Med. (Berl.) 98, 1659–1673.
- [9] Morais, I.J., Polveiro, R.C., Souza, G.M., Di Bortolin, Sassaki, F.T., et al., 2020. The global population of SARS-CoV-2 is composed of six

- major subtypes. Sci. Rep. 10, 18289.
- [10] Cottam, E.M., Whelband, M.C., Wileman, T., 2014. Coronavirus NSP6 restricts autophagosome expansion. Autophagy 10, 1426–1441.
- [11] van der Hoeven, B., Oudshoorn, D., Koster, A.J., Snijder, E.J., Kikkert, M., et al., 2016. Biogenesis and architecture of arterivirus replication organelles. Virus Res. 220, 70–90.
- [12] Zhang, J., Lan, Y., Sanyal, S., 2020. Membrane heist: coronavirus host membrane remodeling during replication. Biochimie 179, 229–236.
- [13] Santerre, M., Arjona, S.P., Allen, C.N., Shcherbik, N., Sawaya, B.E., 2020. Why do SARSCoV-2 NSPs rush to the ER? J. Neurol. 1–10
- [14] De Gordon, Jang, G.M., Bouhaddou, M., Xu, J., Obernier, K., et al., 2020. A SARS-CoV-2 protein interaction map reveals targets for drug repurposing. Nature 583, 459–468.
- [15] Lubin, J.H., Zardecki, C., Dolan, E.M., Lu, C., Shen, Z., et al., 2020. Evolution of the SARS-CoV-2 Proteome in Three Dimensions (3D) during the First Six Months of the COVID-19 Pandemic. bioRxiv.
- [16] Edache EI, Uzairu A, Mamza PA, Shallangwa GA. QSAR, homology modeling, and docking simulation on SARS-CoV-2 and pseudomonas aeruginosa inhibitors, ADMET, and molecular dynamic simulations to find a possible oral lead candidate. J Genet Eng Biotechnol. 2022 Jun 17:20:88.
- [17] E.I. Edache, A. Uzairu, P.A. Mamza, G.A. Shallangwa Theoretical investigation of the cooperation of iminoguanidine with the enzymesbinding domain of covid-19 and bacterial lysozyme inhibitors and their pharmacokinetic properties Journal of the Mexican Chemical Society, 66 (4) (2022), pp. 513-542
- [18] Bioinformatics approach for structure modeling, vaccine design, and molecular docking of Brucella candidate proteins BvrR, OMP25, and OMP31 https://doi.org/10.1038/s41598-024-61991-7
- [19] Applications of Bioinformatics on Genomics and Proteomics Levels Highlighted in Brucella Pathogen 10.21608/jcvr.2024.352697
- [20] McGuffin LJ, Bryson K, Jones DT. The PSIPRED protein structure prediction server. Bioinformatics. 2000 Apr;16(4):404-5.
- [21] Heo, L., Feig, M., 2020. Modeling of Severe Acute Respiratory Syndrome Coronavirus 2 (SARS-CoV-2) Proteins by Machine Learning and Physics-Based Refiement. bioRxiv.
- [22] Senior, A.W., Evans, R., Jumper, J., Kirkpatrick, J., Sifre, L., et al., 2020. Improved protein structure prediction using potentials from deep learning. Nature 577, 706–710.
- [23] Jumper, J., Evans, R., Pritzel, A. et al. Highly accurate protein structure prediction with AlphaFold. Nature 596, 583–589 (2021).

- [24] Md Hossain Shuvo, Muhammad Gulfam, Debswapna Bhattacharya, DeepRefiner: highaccuracy protein structure refinement by deep network calibration, Nucleic Acids Research, Volume 49, Issue W1, 2 July 2021, Pages W147– W152.
- [25] Colovos C and YeatesTO. Verification of protein structures: patterns of nonbonded atomic interactions, , 1993.
- [26] Bugnon M, Röhrig UF, Goullieux M, Perez MAS, Daina A, Michielin O, Zoete V. SwissDock 2024: major enhancements for small-molecule docking with Attracting Cavities and AutoDock Vina. Nucleic Acids Res. 2024.
- [27] Irwin JJ, Tang KG, Young J, Dandarchuluun C, Wong BR, Khurelbaatar M, Moroz YS, Mayfield J, Sayle RA. ZINC20-A Free Ultralarge-Scale Chemical Database for Ligand Discovery. J Chem Inf Model. 2020 Dec 28;60(12):6065-6073.
- [28] Clark, A.M.; Labute, P. 2D depiction of protein—ligand complexes. J. Chem. Inf. Model. 2007, 47, 1933–1944.
- [29] Kutzner C, Pall S, Fechner M, et al. More bang for your buck: improved use of GPU nodes for GROMACS 2018. J Comput Chem 2019;40:2418–31.
- [30] Huang J, Rauscher S, Nawrocki G, et al. CHARMM36m: an improved force field for folded and intrinsically disordered proteins. Nat Methods 2017:14:71–3.
- [31] Vanommeslaeghe K, Raman EP, MacKerell AD, Jr. Automation of the CHARMM general force field (CGenFF) II: assignment of bonded parameters and partial atomic charges. J Chem Inf Model 2012;52:3155–68.
- [32] Darden T, York D, Pedersen L. Particle mesh Ewald: an N·log(N) method for Ewald sums in large systems. J Chem Phys 1993;98:10089–92.
- [33] Bussi G, Donadio D, Parrinello M. Canonical sampling through velocity rescaling. J Chem Phys 2007;126: 014101.
- [34] Parrinello M, Rahman A. Crystal structure and pair potentials: a molecular-dynamics study. Phys Rev Lett 1980;45:1196–9.
- [35] Singh R, Meena NK, Das T, et al. Delineating the conformational dynamics of intermediate structures on the unfolding pathway of beta-lactoglobulin in aqueous urea and dimethyl sulfoxide. J Biomol Struct Dyn 2019;1–10.
- [36] Prakash A, Dixit G, Meena NK, et al. Elucidation of stable intermediates in urea-induced unfolding pathway of human carbonic anhydrase IX. J Biomol Struct Dyn 2018;36(9):2391–406.
- [37] Laberge M, Yonetani T. Molecular dynamics simulations of hemoglobin A in different states and bound to DPG: effector-linked perturbation of tertiary conformations and HbA concerted

- dynamics. Biophys J 2008;94:2737-51.
- [38] Prakash A, Kumar V, Banerjee A, et al. Structural heterogeneity in RNA recognition motif 2 (RRM2) of TAR DNA-binding protein 43 (TDP-43): clue to amyotrophic lateral sclerosis. J Biomol Struct Dyn 2020;1–11.
- [39] Prakash A, Kumar V, Meena NK, et al. Elucidation of the structural stability and dynamics of heterogeneous intermediate ensembles in unfolding pathway of the N-terminal domain of TDP-43. RSC Adv 2018;8(35):19835–45
- [40] Prakash A, Luthra PM. Insilico study of the A(2A)R-D (2)R kinetics and interfacial contact surface for heteromerization. Amino Acids 2012;43:1451–64.
- [41] Wang E, Sun H, Wang J, et al. End-point binding free energy calculation with MM/PBSA and MM/GBSA: strategies and applications in drug design. Chem Rev 2019;119:9478–508.
- [42] Batt SM, Jabeen T, Bhowruth V, et al. Structural basis of inhibition of mycobacterium tuberculosis DprE1 by benzothiazinone inhibitors. Proc Natl Acad Sci U S A 2012;109:11354–9.
- [43] Sastry GM, Adzhigirey M, Day T, et al. Protein and ligand preparation: parameters, protocols, and influence on virtual screening enrichments. J Comput Aided Mol Des 2013;27:221–34.
- [44] Wang C , Nguyen PH , Pham K, et al. Calculating protein-ligand binding affinities with MMPBSA: method and error analysis. J Comput Chem 2016;37:2436–46.
- [45] Ravikumar, Y.; Koonyosying, P.; Srichairatanakool,S.; Ponpandian, L.N.; Kumaravelu, J.; Srichairatanakool, S. In Silico Molecular Docking and Dynamics Simulation Analysis of Potential Histone Lysine Methyl Transferase Inhibitors for Managing β -Thalassemia. Molecules 2023, 28,7266.
- [46] Banerjee P, Kemmler E, Dunkel M, Preissner R. ProTox 3.0: a webserver for the prediction of toxicity of chemicals. Nucleic Acids Res. 2024 Jul 5;52(W1):W513-W520.
- [47] Kyle Swanson, Parker Walther, Jeremy Leitz, Souhrid Mukherjee, Joseph C Wu, Rabindra V Shivnaraine, James Zou, ADMET-AI: a machine learning ADMET platform for evaluation of largescale chemical libraries, Bioinformatics, Volume 40, Issue 7, July 2024, btae416,